Investigating the influence of neighbouring structures on natural ventilation potential of a full-scale cubical building using time-dependent CFD

Article

Published Version

It is advisable to refer to the publisher's version if you intend to cite from the work. See Guidance on citing.

www.reading.ac.uk/centaur

CentAUR

Central Archive at the University of Reading

Reading's research outputs online

Investigating the influence of neighbouring structures on natural ventilation potential of a full-scale cubical building using time-dependent CFD

CrossMark

Marco-Felipe King [a,*], Hannah L. Gough [b], Christos Halios [b], Janet F. Barlow [b], Adam Robertson [c], Roger Hoxey [c], Catherine J. Noakes [a]

[a] Institute for Public Health and Environmental Engineering, School of Civil Engineering, University of Leeds, Leeds, LS2 9JT, UK
[b] Department of Meteorology, University of Reading, Earley Gate, Reading, RG6 6BB, UK
[c] Civil Engineering, School of Engineering, University of Birmingham, Edgbaston, Birmingham, B15 2TT, UK

ABSTRACT

Building location and orientation with respect to incident wind angle are important parameters in determining wind-driven natural ventilation. Experimentally measured façade pressures and ventilation rates in the Silsoe cube under single-sided and cross-flow ventilation configurations are compared with CFD simulations conducted in OpenFoam and ANSYS Fluent using a typical linear workflow approach. Eight wind directions are studied with the cube in isolation and in a new staggered nine cube array format. Comparison is made using CIBSE's prescribed ventilation calculation method based on internal/external building pressure differences. Ventilation rate in the isolated cube with single-sided opening was comparatively lower than either of the cross-flow cases, and relationships between air change rate and wind angle were much weaker in the array cases. For the single opening case with the isolated cube, ventilation effectiveness decreases as the wind turns towards the opening due to increased short-circuiting of airflows. Turbulent structures close to windows improve mixing in the array case. Simulations suggest that vortex shedding from up-wind buildings provides pulsating ventilation in both window configurations, which may attenuate the negative effects of upwind flow obstruction.

1. Introduction

Naturally-ventilated buildings are common worldwide and are advocated as part of sustainable and resilient infrastructure development (Fitzgerald and Woods, 2010). Predicting natural ventilation potential is imperative to understanding building air quality and occupant comfort (Wang et al., 2008). However, natural ventilation flows are complex, driven by a combination of wind and thermal effects. In the case of wind-driven flows, investigated in this paper, the building geometry, openings and orientation with respect to wind-direction are all key parameters. In urban environments the presence of neighbouring buildings also has a significant effect on the local flow field and hence the ventilation potential.

Traditionally, during the design stage of large buildings, scale models (including some surrounding buildings) are placed in a wind tunnel and the pressure distributions around the building measured for various incident wind directions. The resulting pressure coefficients can then be used to calculate the flow through ventilation opening at different locations on the façade, using orifice equations to relate flow rate to wind

speed (CIBSE, 2015). Such approaches are also used to produce generic pressure coefficient data for different building geometries that are published in design guidance (CIBSE, 2015) and can be used to carry out ventilation calculations. These scale-model approaches rely on several assumptions and uncertainties surrounding pressures (Chiu and Etheridge, 2007; Chu et al., 2009; Rahman et al., 2010). Even for a simple building geometry, wind-induced flows can be complex and transient (Coceal et al., 2006), and therefore predicting ventilation rates is difficult (Richards et al., 2007). The relationship between external and indoor airflow is still an area of much debate around appropriate ventilation prediction strategies (Liddament, 1996) and challenging research due to the lack of full-scale building data (Blocken, 2014).

For complex modern buildings, computational fluid dynamics (CFD) simulations of external flows are increasingly used alongside empirical calculations to inform ventilation design. In designing naturally ventilated buildings which are both energy efficient and provide effective ventilation, it is highly desirable to be able to use these simulation approaches to understand the detail of flow patterns and assess both external airflows and the resulting internal ventilation flows inside

---

* Corresponding author.
E-mail address: m.f.king@leeds.ac.uk (M.-F. King).

buildings. However CFD studies also often involve significant approximation and can lead to incomplete understanding of indoor air quality, air change rates, effectiveness and external airflow structures (Fisk et al., 1997; Karava et al., 2011; Larsen and Heiselberg, 2008; Sandberg and Sjöberg, 1983; Sundell et al., 2011). There are currently uncertainties regarding the appropriateness of different CFD codes, and there is a lack of validation at full scale, particularly for coupled external and internal flow in arrays of buildings. As far as the authors are aware, internal air mixing effectiveness has not been studied in relationship to wind angle at full-scale.

In the current study we present a comparison of two widely used computational fluid dynamics (CFD) codes, OpenFoam (v2.3.1 OpenCFD Ltd) and ANSYS Fluent 16 (ANSYS, Canonsburg, PA, USA), against full-scale experimental data collected at the Silsoe cube test facility. The study considers an isolated cube and an irregular nine-cube array to investigate façade pressures, natural ventilation rates and internal mixing. The paper simulates external airflows and wind-driven ventilation within the cube, exploring the influence of wind speed, wind angle and the effect of neighbouring structures on internal mixing for both single-sided and cross ventilation scenarios. The specific objectives of this study are:

- To produce a relationship between incident wind angle and ventilation rate for a cubical structure with openable façade elements in isolation and in an array
- To assess the effect of single-sided opening and cross-flow configurations on ventilation potential
- To assess the effect of all of the above on internal air mixing effectiveness

2. Background

Airflow around bluff bodies resembling buildings has been the subject of a significant body of research to explore airflow in the urban environment. To date, a large number of wind-tunnel experiments and computational modelling studies have been undertaken to try to characterise the airflow patterns and façade pressures around different configurations of blocks to represent buildings in an urban setting (Allegrini et al., 2015; Carpentieri and Robins, 2015; Castro and Robins, 1977; Coceal et al., 2006; Leonardi and Castro, 2010; Richards et al., 2007; Wen et al., 2017; Xie and Castro, 2009). Regular arrays of solid blocks of different aspect ratios (width:height, 1:1, 1:2, 2:1) are typically used in conjunction with varying packing densities in an effort to characterise urban turbulence (Allegrini et al., 2015; Carpentieri and Robins, 2015; Coceal et al., 2006; Leonardi and Castro, 2010) and pollutant dispersion (Gousseau et al., 2011; Gu et al., 2011; Xie and Castro, 2009, 2006a; Yu and Thé, 2016). However, irregular array formations are gaining preference due to their truer representation of urban layouts (Blocken, 2015; Gu et al., 2011; Lin et al., 2014; Xie and Castro, 2006a, 2006b).

Flow through cubical buildings with varying aperture sizes and locations have also been carried out both numerically and in the wind-tunnel (Castro et al., 2017; Karava et al., 2011; Karava and Stathopoulos, 2011; Perén et al., 2015; Tominaga and Blocken, 2016, 2015). However most consider only a few wind angles such as 0°, 90° and 45° and so may miss some important features or trends at angles in between (Richards and Hoxey, 2012) (Afshin et al., 2016). Previous wind-tunnel studies of isolated cubes recognise the necessity of coupling internal and external flow (Tominaga and Blocken, 2016, 2015), however buildings in an urban environment are typically not located in isolation and so the effects of neighbouring structures must also be taken into consideration. More recently, computational modelling studies (Coceal et al., 2006; Gousseau et al., 2011; Hooff and Blocken, 2012; Xie and Castro, 2009, 2006a) have incorporated urban roughness elements and the surrounding buildings within an urban environment.

While there are numerous studies conducted at small-scale, there are far fewer full-scale experimental studies despite the need to capture the variability present in real environments. There is a significant body of work carried out on isolated buildings using the "Silsoe cube" which represents a full-scale idealised experimental scenario that has been used for wind engineering research since the early 1990's (Hoxey and Richards, 1993). Located in an open-country exposed position, the cube has been used for a variety of purposes including pollutant emissions and dispersal, wind loading and also ventilation. Richards and Hoxey have published extensively on external flows around the cube including the phenomenon of flow reattachment (2006), the effect of façade pressure (2001) and wind loading compared to 1:40 wind-tunnel models (2007). Full-scale ventilation studies using the cube were carried out by Straw and subsequently Yang (2004) with a variety of cross-ventilated openings and opening sizes; both authors also carried out steady-state CFD modelling. Studies considering arrays of buildings at full-scale are very limited (Belleri et al., 2014; Dutt et al., 1992; Sawachi et al., 2004). Some examples of 1:5 and 1:50 arrays of cubical structures have been studied at the Comprehensive Outdoor Scale Model (COSMO) (Inagaki and Kanda, 2008) and the Mock Urban Setting Test (MUST) (Biltoft, 2001) but whose primary goal was to study pollutant dispersion and did not investigate wind induced façade pressures. The full-scale experiments conducted in a cube array in the current paper therefore add significantly to the body of work in the field of characterising buildings in urban areas.

Modelling natural ventilation in buildings using CFD, even under isothermal conditions, is complicated. High Reynolds numbers in wind engineering applications require substantially fine grid resolutions in particular in the near-wall regions; which in turn necessitates accurate wall functions (Blocken, 2014). The complex nature of the three dimensional flow field include impingement, separation and vortex shedding and occur frequently in the urban environment. As a consequence, the numerical difficulties associated with flow at sharp corners upstream and resultant problems for discretisation schemes can have significant impact on buildings downstream (Allegrini et al., 2015; Carpentieri and Robins, 2015). Capturing and characterising urban flow features which can directly impact on building ventilation rates or pedestrian comfort depend critically on the ability to model turbulence. Artefacts such as vortex shedding, recirculation and reattachment (Richards and Hoxey, 2006) are commonplace in the urban environment and are well known to pose difficulties to traditional CFD turbulence modelling practices of Reynolds' Averaged Navier-Stokes (RANS) (Gousseau et al., 2011). Despite known inaccuracies (King et al., 2013; Perén et al., 2015; Richards and Norris, 2011), indoor air modelling relies heavily on eddy viscosity k-ε turbulence closure models because of their computationally inexpensive two-equation approach (Evola and Popov, 2006). External flow warrants a time-dependent approach and highly computationally expensive large eddy simulation (LES) models have the ability to capture key flow structures (Carpentieri and Robins, 2015; Lim et al., 2009; Yang, 2004). The necessity for coupling indoor and outdoor airflow simulations for naturally ventilated buildings is becoming increasingly clear, and hence understanding appropriate turbulence models is critical for reliable models.

3. Full-scale Silsoe cube experimental methodology

Experiments were conducted using the Silsoe cube, a 6 m × 6 m × 6 m hollow metallic cube located in a rural location (52.0080° N, −0.4121° W). Two experimental set-ups were investigated: The isolated cube under single-sided and cross-flow ventilation and an array of nine cubes under the same conditions. Fig. 1a shows a close-up of the Silsoe cube including the locations of façade pressure taps and the position of the opening on the front façade (an identical opening is present on the rear face). Fig. 1b shows the set-up of the array configuration in relation to the main structure. Cylindrical tanks located on the Silsoe site of height 1.5 m are also shown in Fig. 1b. Hay bales were stacked to represent cubical structures of the same size for the surrounding eight cubes. Surface roughness was not characterised but variations in roughness was found not to significantly influence flow field calculations. One building height
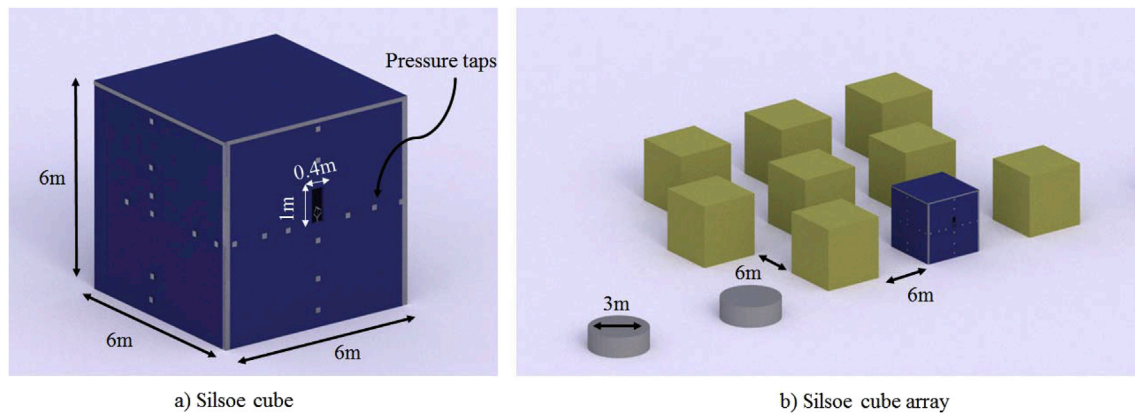
Fig. 1. Experimental set up of the Silsoe cube in isolation and array format.

(1H) gap was left between each cube, with the centre row of cubes offset by 1H (see Fig. 1b.

South-westerly winds dominated throughout the experimental phase and only neutral conditions with moderately high wind speeds (>6 m/s at 6 m) were considered in the analysis. This choice is due to two factors: (i) It was found that the cube tended to heat up on days with strong solar gains, thereby potentially affecting airflow patterns. Thermal effects have been shown to be negligible under neutral conditions (Coceal et al., 2006) and so isothermal CFD simulations could be confidently conducted, representing overcast days. (ii) Calculation of pressure co-efficients are more reliable with wind speeds above 6 m/s (Richards and Hoxey, 2002). Local wind speeds were found to lie predominately in the range 4–10 m/s and so sufficient useful experimental data was collected. For each case eight wind angles were modelled in the simulations based on the prevailing wind at the site as shown in Fig. 2a. The wind rose represents the measured winds during the experimental campaign.

Fig. 3 shows the approach flow parameters assumed in the computational model, based on data previously measured for the Silsoe site by Richards and Hoxey (2002).

3.1. Experimental measurements

Thirty two surface pressure measurements were made using pressure taps (Honeywell, USA.) attached along the centrelines of each of the cube faces, including the roof (see Fig. 1). Sampling was at 10 Hz and averages
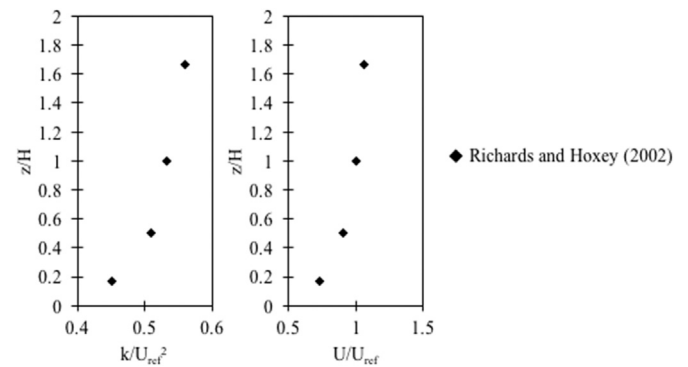

Fig. 3. Site parameters measured in Richards and Hoxey (2002).

were made each 30 min. These instruments and methodologies were chosen as previous studies had conducted measurements at these location and have set a precedent in wind engineering (Richards and Hoxey, 2002). Error was found to be 2.5 cm Hg as stipulated by the manufacturer. Local wind speed and direction was measured at window height (3.5 m) with Gill Instrument Research R3-50 ultrasonic anemometers (Gill Instruments Ltd 2000) at locations 3 m in front (sonic 3) and 3 m behind the cube (sonic 2). Sampling frequency was carried out at 10 Hz and accuracy was found to be <1.0% RMS. A reference velocity was
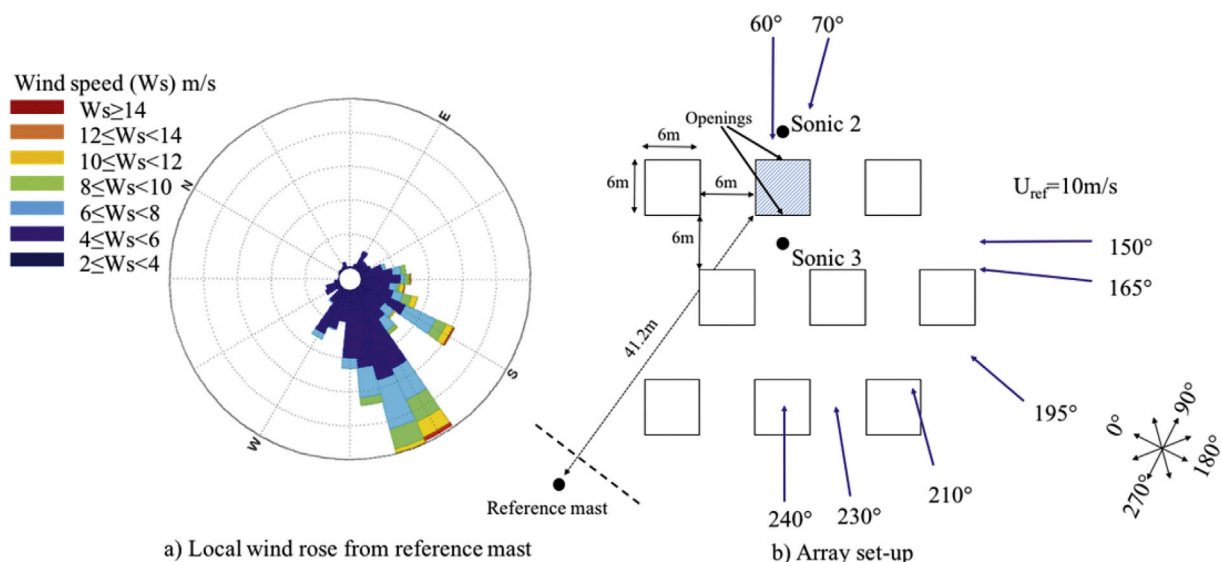

Fig. 2. a) Typical wind directions and speeds, b) wind directions studied.

measured at a mast diagonally upstream of the prevailing WSW wind direction at a height of 6 m (Fig. 2). The authors acknowledge that this reference sonic anemometer, although at a 41 m distance at 45° from the Silsoe cube, may be affected by the turbulent structures in certain wind directions generated by the array cases.

Measurements of wind speeds and façade pressures on the main were made constantly from 30th May 2015 until 7th July 2015. Prominent wind directions measured are 60°, 70°, 150°, 165°, 195°, 210°, 230° and 240° (see Fig. 2). Results are given for specific wind directions and all wind directions are given in meteorological format showing their origin.

3.2. Measurement metrics

Two measurement metrics will be used to compare cases: Calculation of ventilation rate and air change effectiveness.

1. **Ventilation rate:** The Chartered Institution for Building Service Engineers (CIBSE) propose a pressure-based methodology for calculating natural ventilation in buildings by means of an empirical formulation (CIBSE, 2015) using the average façade pressure coefficients (C_p):

$$C_p = \frac{\Delta P}{\frac{1}{2}\rho U_{ref}^2} \qquad (1)$$

Here ΔP is the pressure difference in Pascals between an upwind position and the façade, ρ is fluid density (kg/m^3) and U_{ref} represents a wind reference speed (m/s) at a determined height, typically the building eaves. Infiltration flow rate through a single-sided open façade is then nominally calculated based on window opening area A and an experimentally obtained coefficient of discharge C_d of 0.658 for the current opening:

$$Q = A C_d \sqrt{\frac{2\Delta P}{\rho}} \qquad (2)$$

Flow rates for buildings with wind-induced cross-ventilation occur due to static pressure difference across openings in the building (Karava et al., 2011) and when both openings are the same area, flow rates are given by:

$$Q = \frac{1}{\sqrt{2}} C_d A U_{ref} \sqrt{C_{p_w} - C_{p_l}} \qquad (3)$$

Here C_{p_w} is the pressure coefficient on the windward wall and C_{p_l} is the equivalent on the leeward wall.

Finding accurate and appropriate Cp values both experimentally or numerically has been difficult historically as aspects of the building such as its geometry, sheltering and façade details may alter values (Cóstola et al., 2009). Significant effort has been made to collate databases of façade Cp values for varying conditions and building exposures. As a result, these are used extensively in building energy simulations and airflow network tools currently used both in academia and in industry. Examples of such are: CONTAM, EnergyPlus and ESP-r (Cóstola et al., 2009).

Within the current study, pressures from the four pressure taps around the front and rear windows are used to calculate the C_{p_w} and C_{p_l} respectively from the experimental data. This approach is used with the reference wind speed to calculate the ventilation rate using equation (3) for cross-flow cases. Where the wind is parallel to the cube openings, theoretically, no net pressure difference exists across the whole building. When this is the case, the formulation given by equation (2) was used, which takes into account only the internal (around the window inside) and external pressure differences at the front face of the cube. Comparable values are calculated from the CFD simulation results using the surface pressures on the front and rear faces, and inside the cube as appropriate. In all cases the calculated ventilation rates are presented as normalised values $Q^* = Q/(A U_{ref})$.

2. **Air change effectiveness:** This parameter is calculated from the CFD results to compare internal mixing patterns for different wind directions and ventilation scenarios. It is defined as the ratio between the average age of room air if it were fully mixed, and the average of the age of air at the breathing height (Federspiel, 1999): This was carried out by investigating local age of air, defined as the mean time that it takes a particle to travel from an inlet point, such as the supply opening, to the measurement point. Sandberg and Sjöberg (1983) defined a ventilation performance measure called relative air diffusion efficiency as the ratio of the nominal time constant to the mean age of air and was later renamed air-exchange efficiency or effectiveness.

$$E = \frac{Average\ local\ age\ of\ air\ at\ 1.5\ m}{Average\ overall\ age\ of\ air}, \qquad (4)$$

4. Computational fluid dynamics methodology

Simulations were carried out for the two full-scale geometries: Case 1 isolated cube with single and cross-ventilation (see Fig. 4 a–b) and Case 2: A nine cube array. To position the geometry, horizontal inhomogeneity in the vertical plane was first investigated by performing a simulation on an empty domain to establish appropriate location of the cube(s). It was found that three building heights from the inlet was sufficient to reduce decay of turbulent properties in the approach flow. A domain of (20 m × 50 m × 18 m) was therefore modelled with approximately 3H (building heights) upstream and 5H downstream (Blocken et al., 2007) for the mesh sensitivity analysis and for Case 1. For Case 2 a bounding box of 12H × 16.6H × 6H (72 m × 90 m × 36 m) was used to account for larger size of the array.

As highlighted in section 2, appropriate turbulence model selection is a key consideration. Detached Eddy simulations (DES) offer a hybrid approach between RANS and LES, where regions near solid boundaries and where the turbulent length scale is less than the maximum grid dimension are assigned the RANS mode of solution. The model then switches to a sub-grid scale formulation in regions fine enough for LES calculations (Spalart, 2000). As the turbulent length scale exceeds the grid dimension, the regions are solved using the LES mode. DES are particularly useful because they capture flow features in areas of high separation near the trailing edge of buildings but also benefit from the computationally inexpensive RANS modelling close to the façade. However, DES suffers from possible grid induced separation where flow becomes separated through grid insufficient mesh refinement, leading to inaccurate results (Menter and Egorov, 2010). Scale adaptive simulation (SAS) modelling is an improvement over DES such that the RANS modelling is not influenced by the grid spacing and spurious grid induced separation becomes irrelevant (Menter and Egorov, 2010). Instead of directly relying on grid scales, the SAS approach switches between models dictated by the von Karman length-scale ($L = \kappa \left| \frac{\overline{U}'}{\overline{U}''} \right|$). $\overline{U}'$ and $\overline{U}''$ represent the first and second derivative of velocity in space (Menter and Egorov, 2010). In areas of RANS flow L is large and small in areas of unsteadiness. In regions where the flow is on the limit of going unsteady, the objective of the SAS term is to increase turbulent dissipation (ω). The result is that the turbulent kinetic energy (k) and turbulent viscosity (ν^t) are reduced so that the dissipating (damping) effect of the turbulent viscosity on the resolved fluctuations is reduced, thereby promoting the momentum equations to switch from steady to unsteady mode. Following a turbulence models sensitivity analysis (not published here for reasons of succinctness) this paper utilises the shear-stress turbulence SAS model (SST-SAS) which is based on the model developed by Erogov and Menter (2010). The model was found to give good comparisons against measured surface pressure predictions (see results section), and so is used
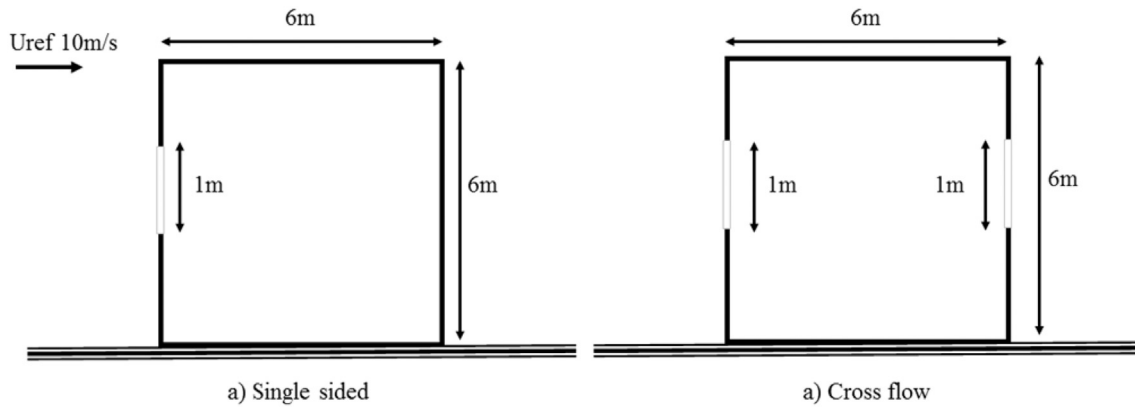
Fig. 4. Vertical central plane through cube (Fig. 1) depicting single-sided and cross-flow opening configuration.

throughout all cases.

4.1. Boundary conditions

Site velocity profile measurements are well matched by a logarithmic profile (equation (5)). In accordance with Richards and Hoxey (2002) we used a reference velocity (U_{ref}) of 10 m/s at z = 6 m and ground roughness length z_0 of 0.01 m to define the inlet velocity condition.

$$\frac{U(z)}{u^*} = \frac{1}{\kappa}\ln\left(\frac{z + z_0}{z_0}\right) \tag{5}$$

Here u^* is the turbulent friction velocity (0.656 m/s) and κ is von Karman's constant (0.41). Reynolds number dependency has been shown to be very weak (Xie and Castro, 2006a), principally because the turbulence production process is at scales comparable to the roughness element sizes. Consequently, a single representative wind speed is used (10 m/s at 6 m). A typical approach to modelling variation in kinetic energy with height was introduced by equation (6). The specific dissipation rate ε (equation (8)) is based on the turbulent dissipation rate (equation (7)) which are standard formulations (Tominaga and Stathopoulos 2011). Equation (8) represents the specific dissipation rate ω, that is required for the k-ω SST SAS simulation method.

$$k = \frac{u^{*2}}{\sqrt{C_\mu}}, \tag{6}$$

where C_μ is the eddy viscosity constant of 0.09.

$$\varepsilon = \frac{u^{*3}}{\kappa(z + z_0)}, \tag{7}$$

$$\omega = \frac{\varepsilon}{k\beta^*} \tag{8}$$

where β^* is 0.09.

Ground roughness was modelled as a constant (0.01 m) as the surrounding countryside was mainly meadow or fields with no crops. Sides and top of the domain are modelled as free-slip walls and are far enough away not to impact the flow around the cube; this was tested during a sensitivity analysis (Blocken and Gualtieri, 2012). The downwind outlet was 0Pa gauge pressure in all cases with zero gradient for all other variables.

4.2. Meshing

Domain meshes were created in snappyHexMesh (OpenCFD Ltd, v2.3.1) for the OpenFoam models and for Fluent simulations, ANSYS

Meshing was used, utilising the cutCell assembly meshing function. The third-party mesh conversion tools foamToFluentMesh and fluent3DMeshToFoam were considered and trialled successfully but do not represent a typical workflow for either software and so were not used. Instead, the meshing tool within each code was used to generate grids for sensitivity analysis. In both cases grids were made of entirely hexahedral cells with clustering of cells around the cubes such that a gradient could be achieved. This gave a workable mesh within the capabilities of available RAM (limitations explained subsequently).

A mesh sensitivity analysis, following the standards set out by Roache (1997) was conducted using four successively smaller grid sizes: 0.06H, 0.03H, 0.02H, and 0.01H. It was found that façade pressure coefficients compared best with experimental data from Richards et al. (2001) when cells of 0.06 m thickness were used at the cube surface. This is representative of a mesh size 0.01H, which is slightly smaller than that recommended by Lim et al. (2009). This mesh showed a grid convergence index of less than 5% when comparing velocity fluctuations at the centre point on the side face of the cube (Schwer, 2008), where all coarser meshes fluctuated more. Bulk flow cell size increases up to 0.6 m downstream of the cubes. Final cell counts for isolated cases and array cases were in the region of 4 million and 16 million cells respectively. Fig. 5 shows the typical mesh type for the array case, depicting cell sizes of 0.01H at the cube expanding up to 0.1H further away.

4.3. Solver settings

In both numerical codes, second-order upwind flux difference splitting schemes were applied to convective terms and a central differencing scheme for diffusion terms. For time integration, a central bounded second-order accurate scheme was utilised. A Courant-Friedrichs-Levy
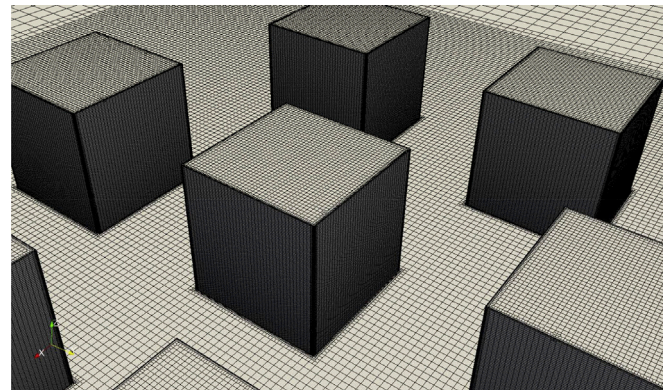

Fig. 5. Mesh created in snappyHexMesh for the parallel flow case. Cells at the cube face are 0.01H with cells far away from the cubes representing 0.1H.

number of 1.6e-1 was used throughout based on $\Delta t = 0.001$, U_{ref} of 10 m/s and $\Delta x = 0.06$ m, which is within the range of best-practice used in transient flow simulations (Nozu et al., 2008; Tominaga et al., 2008). A steady state simulation was run initially to create a starting point for the transient simulation using the SIMPLE pressure-velocity coupling scheme. Pressure interpolation, convective terms and the viscous terms of the governing equations were solved with second order discretisation. The transient simulation, using the PISO scheme, was then run initially for 10 air turnover times without recording results to allow for turbulence structures to form adequately. The results of the simulations were then averaged over 10,000 time steps, which correspond to a flow time of 10s. It is verified that the averaging time is sufficient to obtain statistically steady results by monitoring the evolution of the mean velocity at several locations inside the domain with time using moving averages.

All simulations were conducted at the University of Leeds on 16 Intel Xeon X5650 @ 2.67 GHz cores with 32 GB ECCDDR3 memory.

5. Results

The analysis presented in the following sections examines airflow features important for developing models for natural ventilation analysis. CFD results are post-processed using Paraview 3.8 (Kitware, Inc., USA) and Fluent, respectively.

5.1. External airflow

Fig. 6 shows the mean façade pressure coefficient calculated from 30 min averaged experimental data and both Fluent and OpenFoam simulations based on equation (1). These are plotted along the centreline of the cube with closed windows (i.e. no flow into the cube). Fig. 6 (a) shows the pressure coefficients for the isolated case and Fig. 6 (b) shows the array case. In both cases results are shown with the oncoming wind perpendicular to the cube front face. C_p values published by CIBSE (2015) are superimposed in both cases to compare study results to values used in simple wind ventilation calculations. These are experimentally derived values in wind-tunnel conditions for a variety of wind angles and building sheltering (Liddament, 1986). CIBSE define values for open

country (isolated cube Fig. 5a) and urban location (array of cubes, Fig. 5b). A steady state RANS simulation in Fluent using the k-ω SST turbulence model on the isolated cube same mesh was included for additional comparison.

The results show that for the isolated cube both codes compare well to the experimental data on the front face, but discrepancies appear at reattachment points on the roof where the Fluent model is better able to capture the features present in the experimental data. Both the CIBSE data and the OpenFoam model predict lower values of C_p over the roof. On the rear face, comparison is again fairly good between all approaches, with the Fluent model giving a slightly better result compared to the experiment. The RANS model in the isolated case performs adequately on the front façade but underperforms in comparison to the SAS model on both the roof and the back by 25%. This is a similar finding to Straw et al. (2000).

In the array case, the Fluent model again shows slightly better comparison with the experiment on the front face, but then underpredicts the values of C_p on the rear face. CIBSE data slightly over-predicts the façade pressures in the array case along the front wall and on the roof.

Overall comparison shows that substantial differences exist with respect to the two codes and the experimental values particularly on the roof. It is noted that the pressure contours are not symmetrical because the array is of an irregular shape. Cóstola et al., 2009 show that up to a 50% variation in Cp has been found for the same apparent experiment in different wind tunnels. This underscores how much variation may be expected between simulation and full-scale experiment where uncertainties are much higher. Discrepancies between both codes are due primarily to mesh differences despite all attempts to create these to a similar standard.

5.2. Internal airflow

Fig. 7 shows normalised velocity magnitude ($|U|/U_{ref}$) contours from the OpenFoam simulations plotted on a horizontal plane at window height (3.5 m) for the isolated cube with a cross-flow ventilation configuration. Fig. 8 shows the same for the cube array, also with cross-
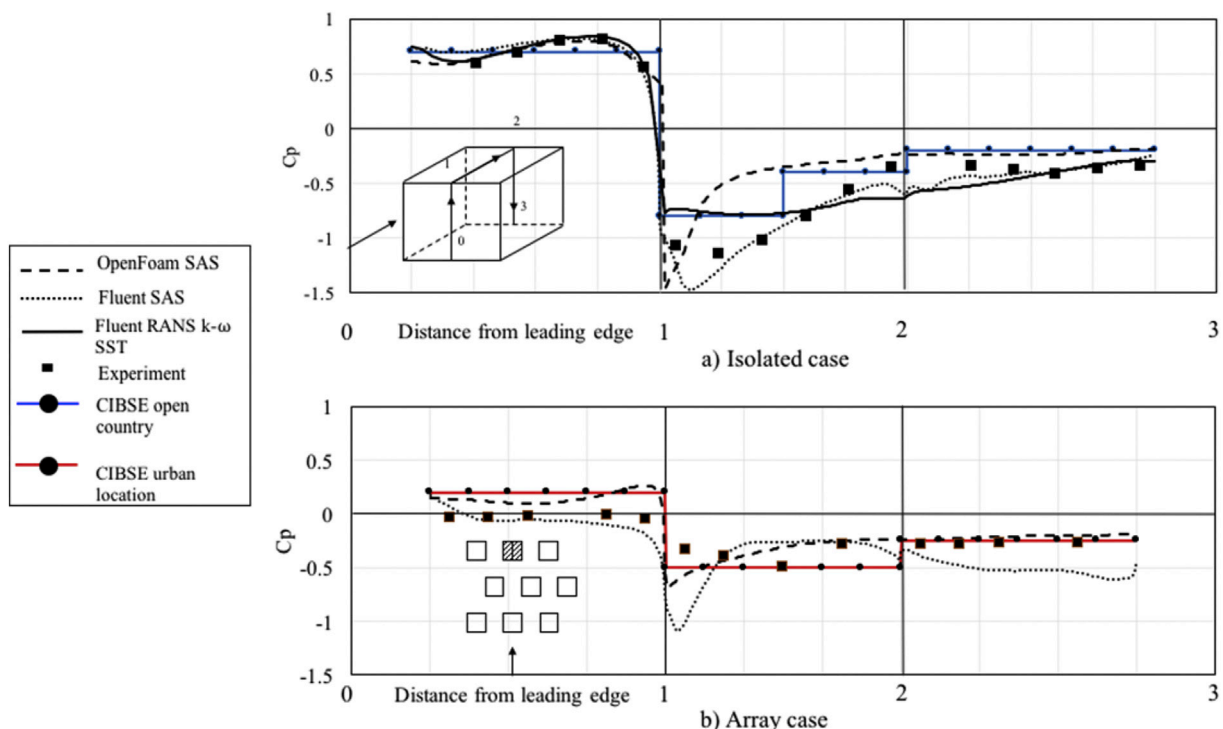

Fig. 6. Comparison of mean pressure coefficient, Cp, for perpendicular wind direction for both isolated (a) and array (b) cases.
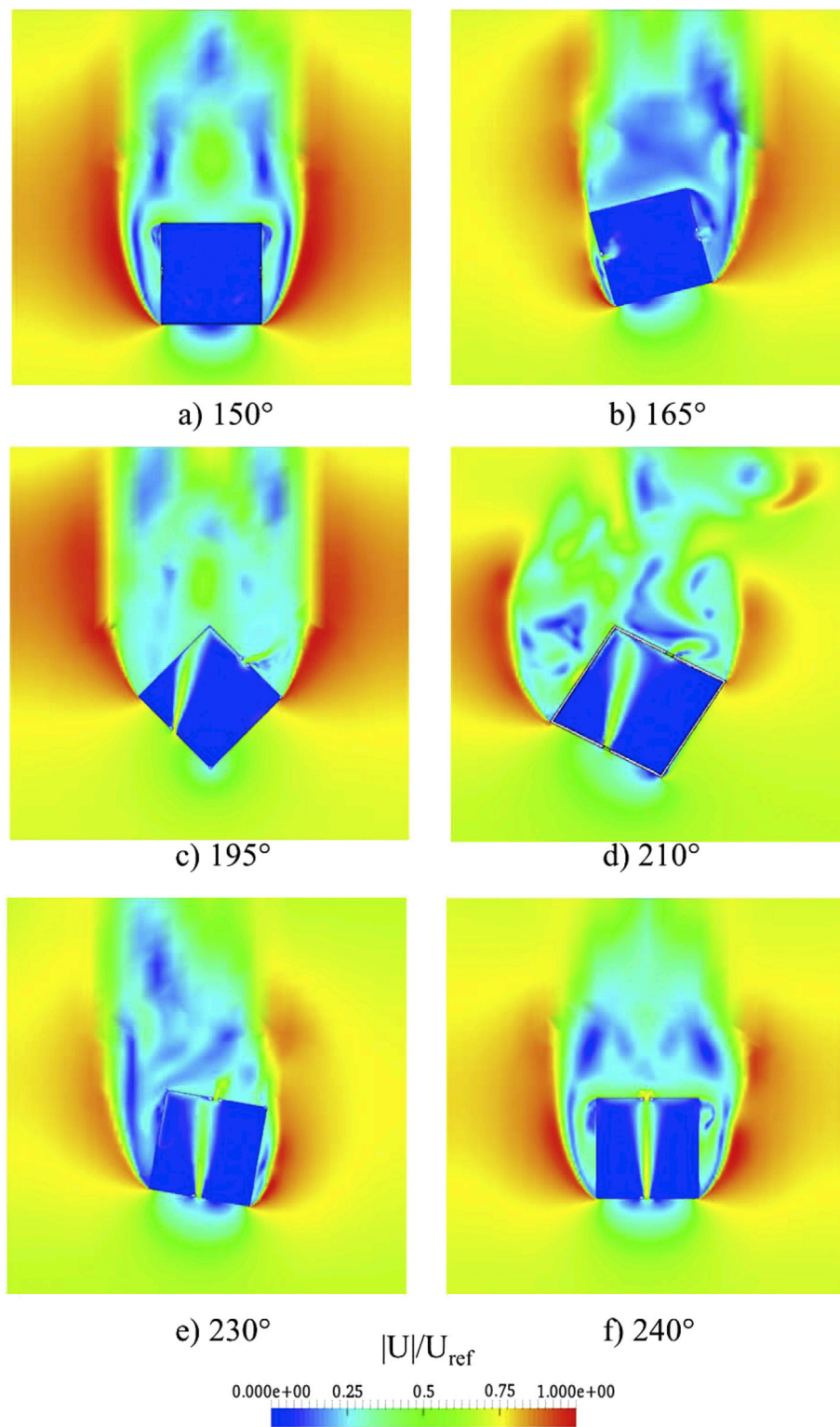
Fig. 7. Isolated cube: Normalised instantaneous velocity magnitude ($|U|/U_{ref}$) on a horizontal plane at window height 3.5 m with cross-flow configuration.

flow configuration. In both cases contours for six wind angles between 150° (parallel to front face) and 240° (perpendicular to front face) are plotted. These are of qualitative interest as they depict the variation in flow characteristics varying by wind angle.

In all cases it can be seen that air speed inside the cube increases as the wind turns towards the window. In the isolated cases (Fig. 7) a pronounced impinging jet phenomenon is observed for all angles above 165°. The results suggest that a critical angle may exist where the diffuse

jet that is dominated by turbulent mixing is replaced by the impinging jets that predominated over angles 180°–240°. Experimental anemometry data supports this feature.

The existence of the impinging jet is not as evident when the cube is surrounded by an array of other cubes (Fig. 8) indicating a shielding effect on the cube from direct wind. As a consequence, even at 240° (perpendicular), only a moderate short jet impingement is seen inside the cube (Fig. 8). In comparison, single-sided ventilation (e.g. Fig. 8) reduces
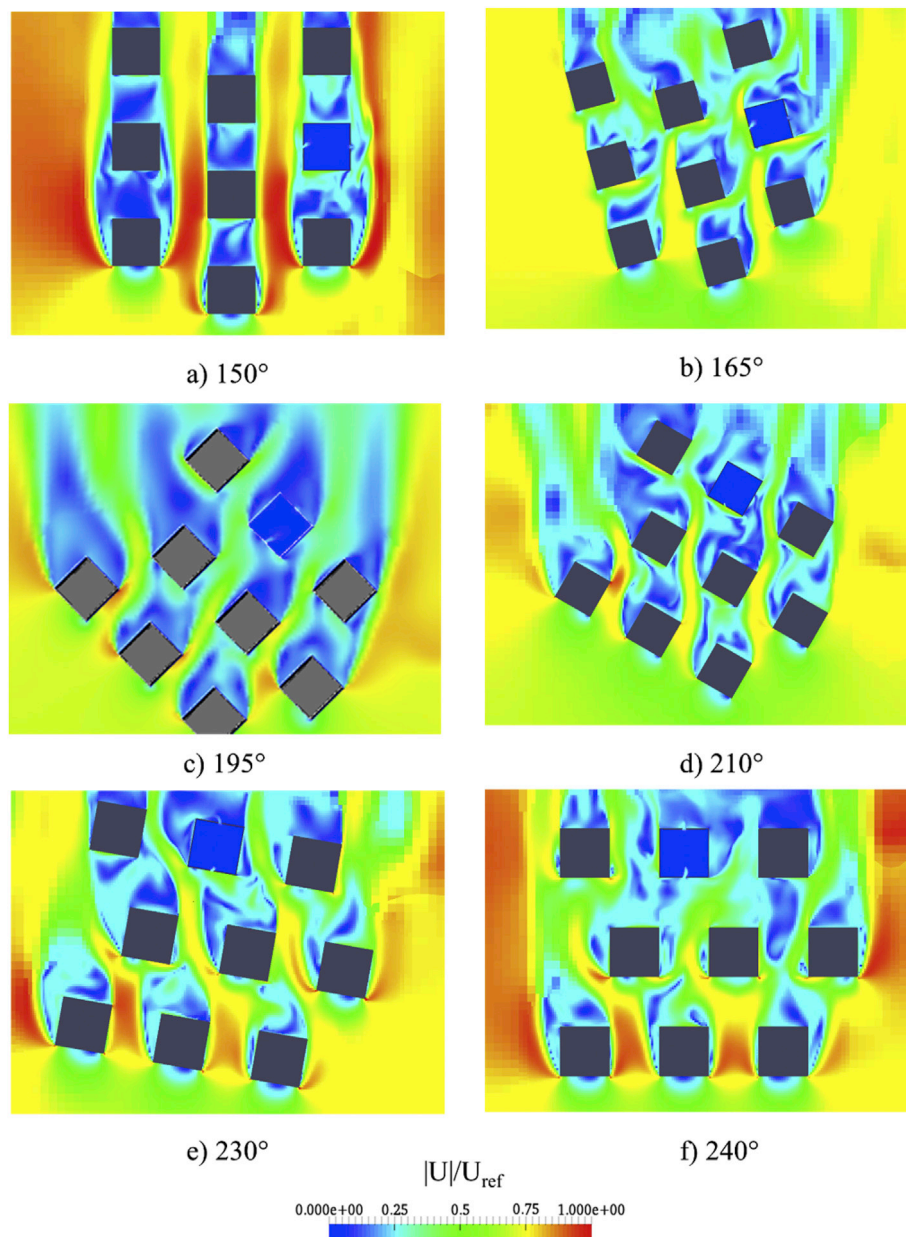
a) 150° b) 165°

c) 195° d) 210°

e) 230° f) 240°

$|U|/U_{ref}$

0.000e+00 0.25 0.5 0.75 1.000e+00

Fig. 8. Normalised instantaneous velocity magnitude ($|U|/U_{ref}$) on a horizontal plane at window height 3.5 m for the cube array with cross-flow configuration.

inflow speeds significantly and the impinging jet phenomenon spanning the entire cube is no longer observed for any case. Instead, the jet decays within 0.25H of the window location regardless of wind direction. Contrary to the cross-flow setting at 240° (Fig. 8), where the impinging jet decays slowest, turbulent decay dominates the inflow patterns in the single-sided case in the isolated location and the jet is shortest of all. A small pulsing phenomenon is found at 150° (Fig. 8) cross-flow when the cube is in isolation, and this becomes magnified in the array case. This is due to strong vortex shedding from up-wind cubes impacting on façade pressures of down-wind cubes. Fig. 9 shows a diffuse jet in the isolated single side 165° case.

5.3. Impact of wind angle on ventilation rate

Fig. 10 shows scatter graphs of normalised air change rate ($Q/(AU_{ref})$) within the cube from experiments and from Fluent and OpenFoam simulations. Experimental values are calculated using equation (2), using the average of four pressure taps around the windward window. Air change

rates are calculated by equation (3) using averages of four pressure taps around the window (see Fig. 1). Error bars on the CFD results represent root mean squared errors either side of the mean. An additional two extra wind directions were also modelled (60° and 70°) in an effort to investigate the effects of symmetry. Results are presented for both cross-flow (Fig. 10 (a), (b), and single-sided (Fig. 11 (a), (b)) ventilation cases.

As the incident wind moves from being parallel to perpendicular to the windows, the air change rate increases for both cross-flow cases (Fig. 10 (a), (b)) and for the isolated cube with single-sided ventilation (Fig. 11a). This is most noticeable in the isolated cross-flow scenario (Fig. 10a). Similar results were found in Chu et al. (2011) for an isolated case. Such patterns are less apparent in the array case (Fig. 11b), where experimentally, a lower ventilation rate and range is found, but computationally a high level of variation is predicted.

The data in Figs. 10 and 11 indicate that similar results are found for both OpenFoam and Fluent simulations, and that both models predict air change rates which are of a comparable magnitude to the experimental results and show the same trends with angle. It was found statistically
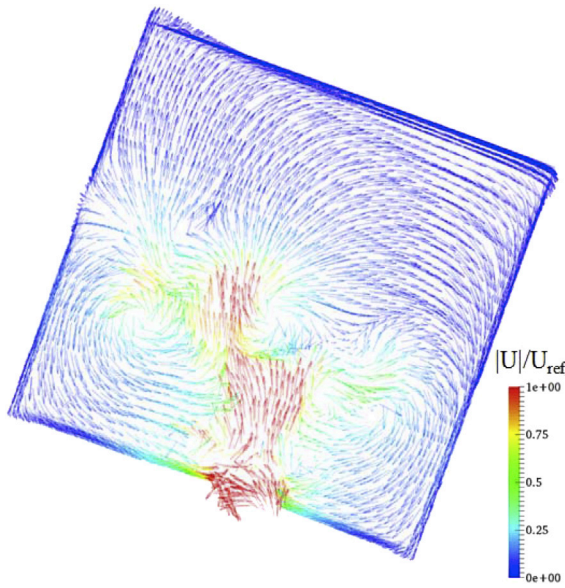
Fig. 9. Snapshot of velocity vectors plotted at 1/2H inside the single-sided ventilated cube at 165°.
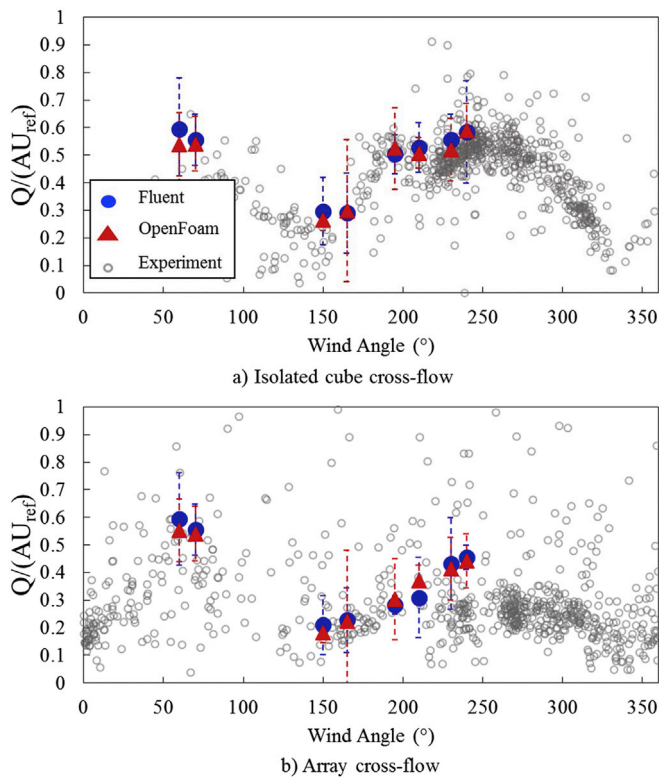

a) Isolated cube cross-flow

b) Array cross-flow

Fig. 10. Comparison of normalised air change rates (Q/(AUref)) for the numerical codes and experiment: Cross-flow.

that no significant difference exists between the trend for the two CFD methods for paired values for all case setups using a non-parametric Wilcoxon rank-sum test. Statistical analysis was also applied to evaluate the relationship between wind direction and ventilation rate; significant correlations (Table 1) were found between wind angle (≥150°) and normalised flow rate (Q/(AU_ref)) in all cases except for the array case with single-sided ventilation.

Across all wind angles, ventilation rates decrease on average by just over 5% between the isolated case and the array configurations for cross-
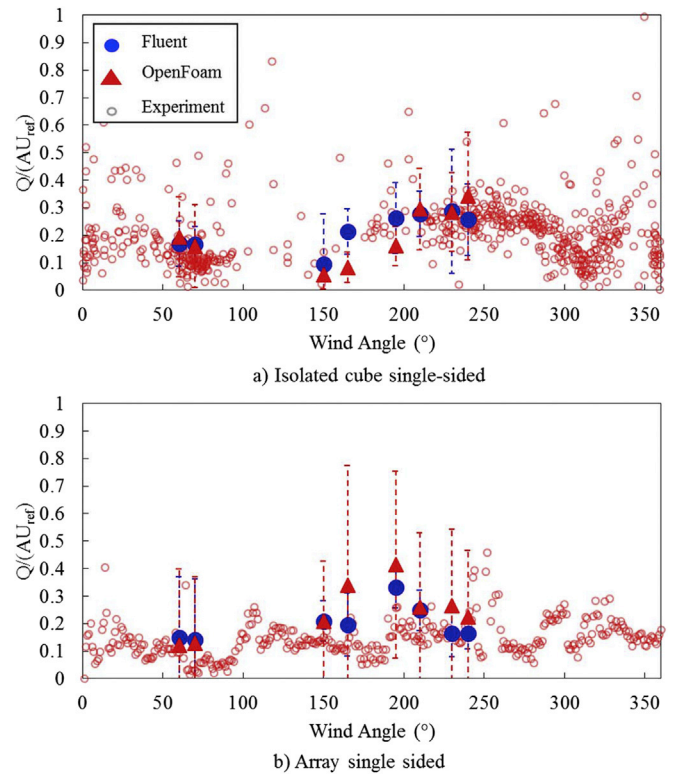

a) Isolated cube single-sided

b) Array single sided

Fig. 11. Comparison of normalised air change rates (Q/(AUref)) for the numerical codes and experiment: Single-sided ventilation.

flow ventilation cases. The single-sided ventilation rate in the isolated cube decreases by 56% compared to the equivalent cross-flow case. Comparatively, ventilation in the single side array case decreases by only 7% vs. the cross-flow ventilated case.

As a comparison for cross-flow, a Silsoe cube study by Straw et al. (2000) with a larger opening (wall-to-window ratio 2.78%) and a similar study by Karava et al. (2011) (wall-to-window ratio 10%) are given in the table (see Table 2) below. In addition, a steady state RANS model using the k-ω SST is added for comparability to the Straw et al. study.

5.4. Impact of wind angle on internal mixing and ventilation effectiveness

Whilst the overall calculated ventilation rates in the cube give an indication of the air exchange rates, analysing the distribution of local ventilation rates throughout each cube is a convenient way of comparing the effect of different angles of approach flow on both overall rate and mixing.

To implement this in the CFD models an additional scalar transport equation was solved in the following form:

$$\nabla \times (\rho u \phi_i) = S_{\phi_i} \qquad (9)$$

where S_{ϕ_i} is the source term of the scalar ϕ_i. E gives a measure of the distribution of air at the breathing height and a value close to unity indicates that the air distribution within the zone has reached perfect mixing. Values less than 1 suggests short-circuiting, where fresh air bypasses the breathing zone. Values greater than 1 suggest areas of stagnation outside the breathing zone.

Figs. 12 and 13 show frequency density plots of air change effectiveness (E) at the breathing height (1.5 m) measured in a sphere 1 m in diameter at the centre of the cube compared to the overall age of air in the cube for the isolated cube and array of cubes respectively. Levels of variation depend on transient flow effects.

The single-sided ventilated cube, both in the isolated and array cases,

Table 1

Linear correlations between angle and air change rate for the two CFD codes. * indicates highly significant correlation (p < 0.05).

Case/ Solver	Isolated Cross-Flow	Isolated Single-Sided	Array Cross-Flow	Array Single-Sided
Fluent	0.67	0.82*	0.89*	None
Openfoam	0.93*	0.95*	0.93*	None

Table 2

Comparison between Cp derived CFD Q/(AU_ref) values are given where available along with a % difference.

	STRAW ET AL. 2000	CURRENT SAS K-W SST	CURRENT RANS K-W SST	Karava et al., 2011
% WALL-WINDOW RATIO	2.78%	1.11%	1.11%	10.35%
EXPERIMENTAL Q/(AU_{REF}) BY CP	0.67	0.54	0.54	0.46
CFD Q/(AU_{REF}) BY CP	0.483	0.59	0.675	–
% DIFFERENCE	27.91%	9.26%	25%	–

shows relatively low levels of variation in air change effectiveness (*E*). E is generally centred on 1 for all wind angles except the 240° isolated case where the value is significantly higher than 1. This suggests that in the majority of cases there is a good degree of mixing in the cube, and that there is little variation with time. Results from the cross-flow ventilation models show relatively high variability throughout, with distribution skewness moving from right to left as the window becomes perpendicular to the wind. As a result, the air change effectiveness presents transitions from mildly recirculating ($E > 1$) to significant short-circuiting ($E < 1$). Analysis of variance, performed between OpenFoam and Fluent predictions of E showed no significant differences ($p > 0.05$) and hence Fluent data are not shown.

6. Discussion

The experimental results show that mean flow structure and turbulence statistics depend significantly on the presence of additional cubes and the wind angle. Unsteady transient effects are important, especially in the lower canopy layer where turbulent fluctuations dominate over the mean flow (Lim et al., 2009). Measurements in a full-scale set-up of this kind are challenging, not least due to the variation of wind direction during averaging periods. The findings are sensitive to slight wind angle changes and therefore significant variation was found for all parameters measured. Approach flow turbulence kinetic energy and velocity magnitudes with respect to vertical height are given in Fig. 3. The authors acknowledge that these can have significant effects on Cp measurements up to 30% as found by Cóstola et al. (2009) however measurement was not available for other wind angles during this experiment.

Both numerical codes applied in the study are able to simulate the pressure coefficients on the façade of the cube in isolation (Fig. 6a) and when other buildings surround it (Fig. 6b). In both cases, the roof presents a complicated area to model due to turbulent shear layers and re-attachment zones, however this is likely to be the least important face for ventilation calculation in most buildings. Skimming flow dominates in the array scenario when the incident flow is at a right angle to the street canyons and can be seen in Fig. 6b to produce comparatively low front-face Cp values.

The amount of sheltering of a building is known to have an impact on the flow structures in the urban canyon, whereby potentially affecting Cp values. The CIBSE guide A acknowledges this by including a sheltering factor in their recommendations; whereby up to a 250% difference is found between isolated and urban scenarios. Fig. 6 compares the effect of building isolation vs. urban sheltering on Cp, and shows up to a 191%

difference between simulated cases, which is in line with Cóstola et al.'s review findings (2009).

The CIBSE (2015) low-rise building Cp values are taken from the AIVC handbook 1986, which were created as a result of a workshop in 1984 (*AIVC. In: Wind pressure workshop proceedings AIC-TN-13.1-84. Brussels: AIVC; 1984.*). These are thought to largely originate from wind-tunnel experiments by Bowen (1976).

CIBSE guide A (2015) provides some insight into varying C_p dependent on the building location but the orifice equation does not account for window thickness or varying façade pressures with height. In fact British Standards EN 1991-1-4 + UK National Annex (NA) (British Standards, 2010) acknowledges the effect of airflow "funnelling" between buildings, stating: "Where the walls of two buildings face each other and the gap between them is less than *e* (where *e* is the lesser of two building dimensions – the cross-wind breadth and twice the height), "funnelling" will accelerate the flow and make the pressure coefficients in zones A (front roof), B (back roof) and C (back) more negative than in the case where the building is "isolated" (British Standards, 2010). When the canyon gap is equal to the building breadth in the cross-wind direction the standards suggest using isolated building C_p values for ventilation calculations.

6.1. Air change rate

For all configurations tested, two distinct indoor flow regimes were found: quasi-impinging jet and recirculation. Ventilation rates were computed using the standard method of pressure differences across the openings. Other authors (Straw et al., 2000) have noted that tracer gas decay calculate would be a more appropriate method, but due to the size of the domain it was too difficult to accurately replicate this method, although it was attempted. In addition, the reader should also bear in mind that the opening in the cube is a hole rather than a window, but could be considered to resemble a vertical casement window. This study is an attempt to show the relationship between wind direction and ventilation potential for a simplified and idealised building, not to predict absolute values for highly complex structures. Therefore, the ventilation rates found here should be treated as conservative estimates.

The opening-to-wall ratio for the current research was 1.11% which is considered small, in comparison to previous Silsoe experiments (2.78% in Straw (2000) and other similar experiments 10% in (Karava et al., 2011). However, it is thought to be more representative of real windows-to-wall ratios for naturally ventilated buildings. Straw (2000) found Q/(AUref) experimentally for a perpendicular wind case to be 0.675 which is slightly higher than the value of 0.54 here. He found that CFD calculations predicted differed by 27.91% vs 9.26% here. In comparison, RANS simulation predictions differed by up to 25% for the current configuration, which may suggest that RANS are less accurate for smaller openings with respect to the windward façade. This is supported by research by van Hoof et al. (2017) that shows that one of the reasons RANS simulations appear useful is because excessive turbulent kinetic energy production outside the cube may be transported inside through large openings. In contrast, when the opening is small, as in the current case, this may not happen. Additionally, Karava et al. (2011) found that potential ventilation values increased in a non-linear fashion for increasing façade opening ratio with Q/(AUref) values ranging from 0.18 to 0.48 depending on the location of the opening on the windward façade.

Single-sided ventilation tends to show comparatively lower air change rates but increased turbulence intensity in the canyon from upwind buildings can improve this (angles >210° Fig. 10a). Van Hoof et al. (2017) show that higher levels of turbulence intensity contribute to jet diffusion, whereby facilitating ventilation and mixing effectiveness.

As the wind turns towards the windows, an impinging jet dominates the indoor flow features for all cross-flow cases. Where the window(s) is parallel to incident flow, turbulent dissipation and recirculation dominate the inflow patterns. In the isolated case, Fluent produces slightly
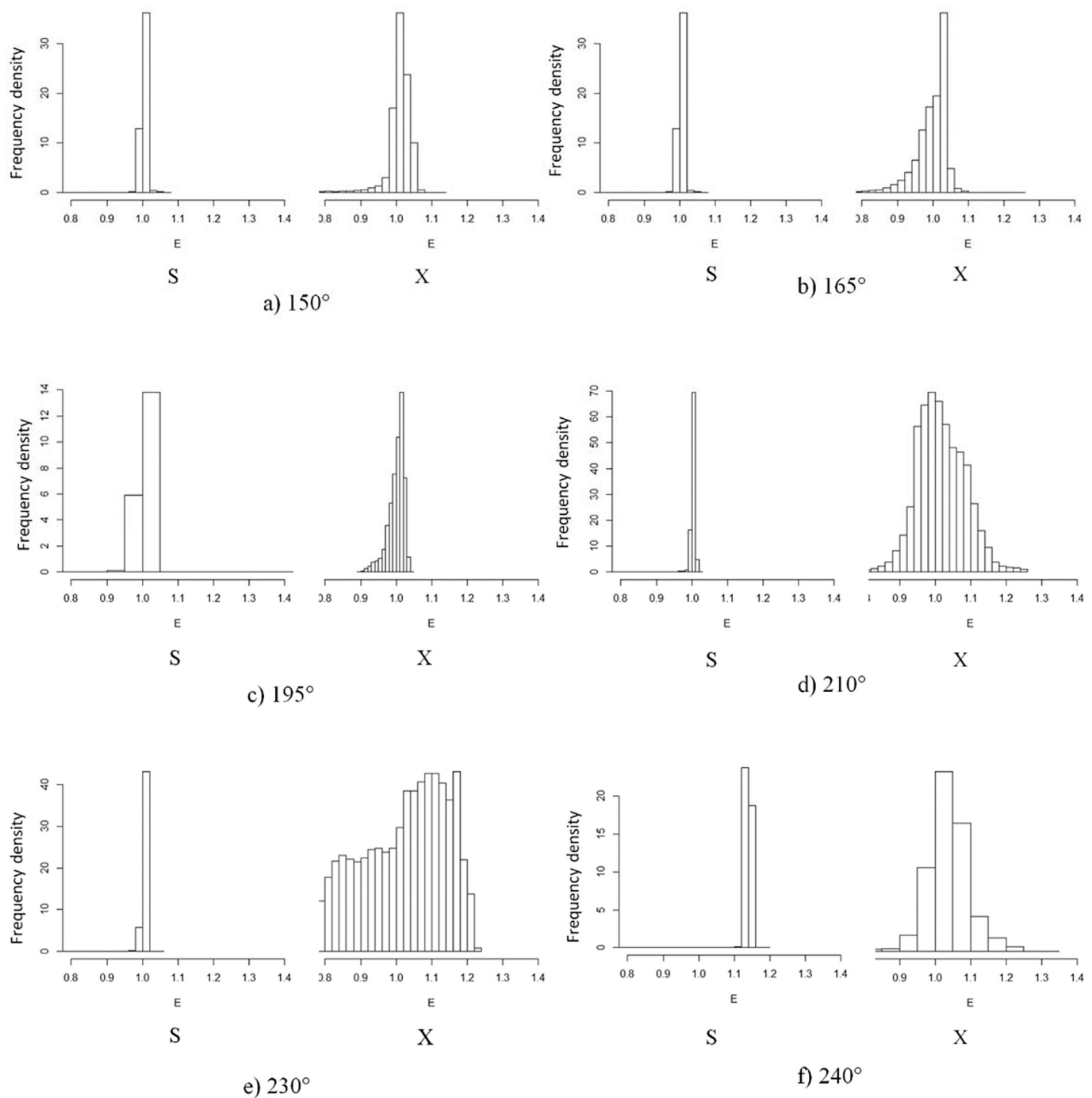
Fig. 12. Frequency distributions of air change effectiveness (E) with wind angle for the isolated cube set-up in OpenFoam, for single-sided (S) and cross-flow(X) ventilation.

higher values than OpenFoam, but still in line with the experimental data. Root mean squared error values are within the same order of magnitude for both solvers. In the single-sided cases in an isolated cube, the inlet jet is at its shortest at wind angle 150°. As the cube has no additional leakage, the window performs as an inlet and an outlet at the same time and hence averaged velocity contours show the inflow air patterns result in a stunted jet, decaying within a metre of the window. Upwind structures block the prominent effects of oncoming wind, in general, causing ventilation rates to drop. Therefore, variations increase in air change rates and these are highly dependent on local turbulent structures.

Fig. 9b shows that cross-flow array cases at angles 60° and 70° exhibit significantly higher ventilation rates than the equivalent in the isolated state (Fig. 9a), suggesting that a blockage effect of neighbouring buildings may increase ventilation rates when the wind is incident to the open window and the building is on the periphery of the array.

When the cross-flow ventilated test building is located at the back of the cubic array, air change rate increases roughly linearly from 150° to 240°. No such strong correlation is found for the single-sided ventilated cube setup. Buildings in central array locations could benefit from cross-flow ventilation to improve air change effectiveness and rely on upwind buildings providing pulsating flow on days when the wind is parallel to the openings.

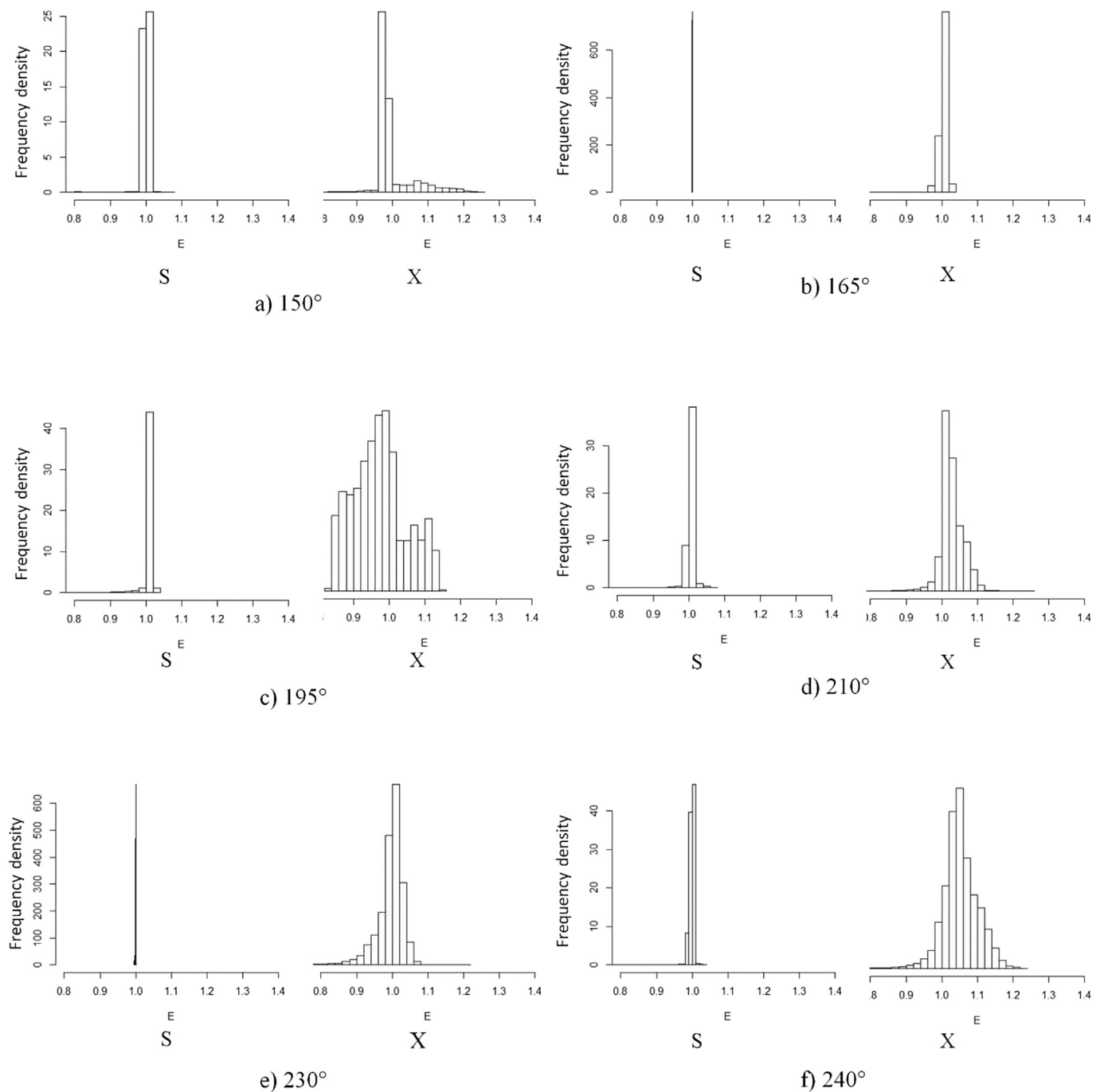When the wind is parallel to the windows (150° cases), upwind

Fig. 13. Frequency distributions of air change effectiveness (E) with wind angle for the array cube set-up in OpenFoam for single-sided (S) and cross-flow(X) ventilation.

buildings provide vortex shedding which appears to induce pulsating ventilation. As a result, little difference is seen between single-sided and cross-flow ventilation in the array setting. Average air change rates between isolated and array cases are comparable but root mean squared errors increase significantly in the latter. Single-sided ventilation can therefore be a valid ventilation method under conditions where wind runs parallel to street canyons.

Differences in prediction between Fluent and OpenFoam may be down, in part, to the way the data is obtained from the model. In order to be replicate experimental practice, an average of four pressures around the window, both inside and outside is used in the calculation of ventilation rate. Fluent natively uses point averages to reproduce values whereas Paraview uses cell-to-point conversion. As a consequence, a 5%

difference has been found to exist so should be added as variation in the root mean squared errors. All efforts were made to make sure the meshes were similar between the two codes in terms of y^+ value and cell sizes, but the intrinsic manner in which each code creates the mesh may contribute to differences found. Mesh conversion utilities such as foamMeshToFluent and fluent3DMeshToFoam were tried successfully in both directions but it was felt that this did not represent a typical CFD workflow pattern. Instead, the native meshing tools of snappyHexMesh and Ansys Meshing were used with their respective codes. Therefore, the results presented in the paper may show a representation for each code individually and can be quantitatively compared. This can highlight to the user, that meshing plays an important part in solution variation between solvers despite specific requirements on y^+ being satisfied.

Other factors may include the effect of wall functions with both solvers being set for high Reynolds number solutions. Within the cube itself, the flow may be found to be comparatively of a much lower Re number and so the solvers may fail to capture certain physics in slow recirculation zones. Inclusion of low-Re wall functions may improve results. Inclusion of more realistic surface roughness and dynamic mesh refinement may allow for increasing approximation between both codes and experimental results, especially for exterior surface pressures.

Instrument measurement accuracy has not been found to influence experimental results significantly. Differences in experimental data for each angle may be attributed to the averaging period (30 minutes) and the angle range for each angle (±2.5°). Despite this, a substantial data set has been accrued, which has shown clear trends in ventilation rates that are matched by the simulations.

6.2. Air change effectiveness

Higher air change effectiveness suggests short circuiting, where the fresh air bypasses the breathing zone. Mean mixing effectiveness in the isolated cube cases is similar for both single-sided and cross-flow cases (Figs. 9 and 11 (S cases)), where the Wilcoxon rank-sum non-parametric statistical test cannot reject the null-hypothesis of similarity (p > 0.05). The presence of neighbouring buildings in the array reduces the mixing effectiveness at breathing height and increases local air residence time, showing that recirculation may exist in the cross-flow cases for wind angles 150°–195°.

On the other hand, mixing appears to decrease as the wind angle increases from 195° to 210° in the cross-flow cases (Figs. 9 and 11 (X cases)). In addition, E increases further for cross-flow cases 230° and 240° as angle increases (p = 0.01).

6.3. Future considerations

At neutral conditions, where buoyancy effects are negligible, heat gain from the sun on cube façades was not included. There would also be further thermal effects arising from heat sources within buildings. In addition, building eaves were excluded as they would include unnecessary complexities to the flow field (Blocken, 2014). However, in simulation of real urban environments both effects may need to be considered. It should also be noted that the cube array does not consider the influence of variable building heights; these will be included in future simulations as they are more representative of an urban environment than cubes of similar sizes (Xie and Castro, 2006a).

7. Conclusion

This paper presents a CFD analysis using Ansys Fluent and OpenFoam software compared against novel experimental measurements of airflow in and around a full-scale cubical structure when in isolation and when within an irregular asymmetrical array. The CFD modelling enabled parametric analysis of wind directions and gives insight into the external flow patterns and effect of internal mixing. The conclusions of the study are as follows:

- This verification study shows that both OpenFoam and Fluent are capable of accurately simulating isothermal flow around isolated cubes and cube arrays. Although meshes differed between solvers, the k-ω SAS model shows to be suitable approach to simulating flow features present within building arrays and enabling external-internal flow coupling, with both solvers giving similar trends.
- Air change rates increase as the incident wind becomes perpendicular to the window for cross-flow cases. This is reflected in both experiment and computation simulation. The isolated cube showed comparatively similar ventilation rates to the array cube at these angles.

- Single-sided ventilation tends to be hard to predict and computational variation is higher. However, only mild discernible decrease in ventilation rates in the array format can be found as the wind turns towards the window.
- For all configurations tested, two distinct flow regimes were found: impinging jet and recirculation. Single-sided ventilation tends to show comparatively lower air change rates but higher turbulence intensity in the canyon appears to improve this (angles >210° Fig. 9).
- Local air change effectiveness within the cube increase as flow aligns with the window showing some short-circuiting for cross-flow ventilation. Similar metrics for single-sided cases remain roughly constant throughout wind angle variations.

The paper is an attempt to investigate simple urban-like geometries at full-scale, where their effects on ventilation can be more easily isolated and therefore better understood. While it is an idealised study, that only considers wind-driven effects, the coupling of irregular asymmetrical arrays, with openable façade elements at full-scale provides a clear opportunity to investigate ventilation under realistic wind conditions. On the basis of the analysis presented above, the study has a number of implications for the design and control of openings in buildings with cross-flow and single-sided ventilation:

- In urban locations, it is insufficient to take C_p values for isolated buildings as accurate representations; it is necessary to include the influence of other buildings. The CIBSE guide A (2015) recommended values for urban locations overestimate the front face C_p and consequently could lead to overestimation of ventilation rate.
- Higher flow rates are observed for cross-flow ventilation with impinging jets being displayed at most wind angles. This in turn reduces air exchange effectiveness as the air short-circuits between the windows.
- Due to the fact that other buildings cause a bottle-neck for wind and the pulsating vortices from upwind structures, buildings on the periphery of an urban location would benefit from single-sided ventilation as a trade-off between lower indoor air speeds and improved local air mixing for any wind angle.
- Buildings in central array locations could benefit from cross-flow ventilation to improve air change effectiveness and rely on upwind surrounding buildings to provide pulsating flow on days when the wind is parallel to the openings. As a disadvantage, higher indoor air speeds may be found. Feasibility will also depend on the building internal design and other considerations such as noise and external air pollution.

Conflicts of interest

None to report.

References

Afshin, M., Sohankar, A., Manshadi, M.D., Esfeh, M.K., 2016. An experimental study on the evaluation of natural ventilation performance of a two-sided wind-catcher for various wind angles. Renew. Energy 85, 1068–1078. http://dx.doi.org/10.1016/j.renene.2015.07.036.

Allegrini, J., Dorer, V., Carmeliet, J., 2015. Influence of morphologies on the microclimate in urban neighbourhoods. J. Wind Eng. Ind. Aerodyn. 144, 108–117. http://dx.doi.org/10.1016/j.jweia.2015.03.024.

Belleri, A., Lollini, R., Dutton, S.M., 2014. Natural ventilation design: an analysis of predicted and measured performance. Build. Environ. 81, 123–138. http://dx.doi.org/10.1016/j.buildenv.2014.06.009.

Biltoft, C., 2001. Customer Report for Mock Urban Setting Test. Defense Threat Reduction Agency Distribution authorized to U.S. government Alexandria.

Blocken, B., 2015. Computational Fluid Dynamics for urban physics: importance, scales, possibilities, limitations and ten tips and tricks towards accurate and reliable simulations. Build. Environ. 91, 219–245. http://dx.doi.org/10.1016/j.buildenv.2015.02.015.

Blocken, B., 2014. 50 years of computational wind engineering: past, present and future. J. Wind Eng. Ind. Aerodyn. 129, 69–102. http://dx.doi.org/10.1016/j.jweia.2014.03.008.

Blocken, B., Gualtieri, C., 2012. Ten iterative steps for model development and evaluation applied to computational fluid dynamics for environmental fluid mechanics. Environ. Model. Softw. 33, 1–22. http://dx.doi.org/10.1016/j.envsoft.2012.02.001.

Blocken, B., Stathopoulos, T., Carmeliet, J., 2007. CFD simulation of the atmospheric boundary layer: wall function problems. Atmos. Environ. 41, 238–252. http://dx.doi.org/10.1016/j.atmosenv.2006.08.019.

Bowen, A., 1976. A Wind Tunnel Investigation Using Simple Building Models to Obtain Mean Surface Wind Pressure Coefficients for Air Filtration Estimates.

British Standards, 2010. UK National Annex to Eurocode 1 – Actions on Structures, Part 1–4: General Actions – Wind Actions. ICS 91.010.30; 93.040.

Carpentieri, M., Robins, A.G., 2015. Influence of urban morphology on air flow over building arrays. J. Wind Eng. Ind. Aerodyn. 145, 61–74. http://dx.doi.org/10.1016/j.jweia.2015.06.001.

Castro, I., Xie, Z., Fuka, V., Robins, A.G., Carpentieri, M., Hayden, P., Hertwig, D., Coceal, O., 2017. Measurements and computations of flow in an urban street system. Boundary-Layer Meteorol. 162, 207–230. http://dx.doi.org/10.1007/s10546-016-0200-7.

Castro, I.P., Robins, A.G., 1977. The flow around a surface-mounted cube in uniform and turbulent streams. J. Fluid Mech. 79, 307–335. http://dx.doi.org/10.1017/S0022112077000172.

Chiu, Y.H., Etheridge, D.W., 2007. External flow effects on the discharge coefficients of two types of ventilation opening. J. Wind Eng. Ind. Aerodyn. 95, 225–252. http://dx.doi.org/10.1016/j.jweia.2006.06.013.

Chu, C.R., Chen, R.H., Chen, J.W., 2011. A laboratory experiment of shear-induced natural ventilation. Energy Build. 43, 2631–2637. http://dx.doi.org/10.1016/j.enbuild.2011.06.014.

Chu, C.R., Chiu, Y.H., Chen, Y.J., Wang, Y.W., Chou, C.P., 2009. Turbulence effects on the discharge coefficient and mean flow rate of wind-driven cross-ventilation. Build. Environ. 44, 2064–2072. http://dx.doi.org/10.1016/j.buildenv.2009.02.012.

CIBSE, 2015. CIBSE GUIDE a: ENVIRONMENTAL DESIGN, seventh ed. CIBSE Publications, London. http://dx.doi.org/10.1016/B978-0-240-81224-3.00016-9.

Coceal, O., Thomas, T.G., Castro, I.P., Belcher, S.E., 2006. Mean flow and turbulence statistics over groups of urban-like cubical obstacles. Boundary-Layer Meteorol. 121, 491–519. http://dx.doi.org/10.1007/s10546-006-9076-2.

Cóstola, D., Blocken, B., Hensen, J.L.M., 2009. Overview of pressure coefficient data in building energy simulation and airflow network programs. Build. Environ. 44, 2027–2036. http://dx.doi.org/10.1016/j.buildenv.2009.02.006.

Dutt, A.J., de Dear, R.J., Krishnan, P., 1992. Full scale and model investigation of natural ventilation and thermal comfort in a building. J. Wind Eng. Ind. Aerodyn. 44, 2599–2609. http://dx.doi.org/10.1016/0167-6105(92)90051-B.

Evola, G., Popov, V., 2006. Computational analysis of wind driven natural ventilation in buildings. Energy Build. 38, 491–501. http://dx.doi.org/10.1016/j.enbuild.2005.08.008.

Federspiel, C.C., 1999. Air-change effectiveness: theory and calculation methods. Indoor Air 9, 47–56.

Fisk, W.J., Faulkner, D., Sullivan, D., Bauman, F., 1997. Air change effectiveness and pollutant removal efficiency during adverse mixing conditions. Indoor Air 7, 55–63. http://dx.doi.org/10.1111/j.1600-0668.1997.t01-3-00007.x.

Fitzgerald, S.D., Woods, A.W., 2010. Transient natural ventilation of a space with localised heating. Build. Environ. 45, 2778–2789. http://dx.doi.org/10.1016/j.buildenv.2010.06.007.

Gousseau, P., Blocken, B., Stathopoulos, T., van Heijst, G.J.F., 2011. CFD simulation of near-field pollutant dispersion on a high-resolution grid: a case study by LES and RANS for a building group in downtown Montreal. Atmos. Environ 45, 428–438. http://dx.doi.org/10.1016/j.atmosenv.2010.09.065.

Gu, Z.-L., Zhang, Y.-W., Cheng, Y., Lee, S.-C., 2011. Effect of uneven building layout on air flow and pollutant dispersion in non-uniform street canyons. Build. Environ. 46, 2657–2665. http://dx.doi.org/10.1016/j.buildenv.2011.06.028.

Hooff, T. Van, Blocken, B., 2012. Air Pollutant Dispersion from a Large Semi-enclosed Stadium in an Urban Area: High-resolution CFD Modeling versus Full-scale Measurements.

Hoxey, R.P., Richards, P.J., 1993. Flow patterns and pressure field around a full-scale building. J. Wind Eng. Ind. Aerodyn. http://dx.doi.org/10.1016/0167-6105(93)90075-Y.

Inagaki, A., Kanda, M., 2008. Turbulent flow similarity over an array of cubes in near-neutrally stratified atmospheric flow. J. Fluid Mech. 615, 101. http://dx.doi.org/10.1017/S0022112008003765.

Karava, P., Stathopoulos, T., 2011. Wind-induced internal pressures in buildings with large façade openings. J. Eng. Mech. Press. http://dx.doi.org/10.1061/(ASCE)EM.1943-7889.0000296, 10, 358–370.

Karava, P., Stathopoulos, T., Athienitis, A.K., 2011. Airflow assessment in cross-ventilated buildings with operable façade elements. Build. Environ. 46, 266–279. http://dx.doi.org/10.1016/j.buildenv.2010.07.022.

King, M.-F., Noakes, C.J., Sleigh, P.A., Camargo-Valero, M.A., 2013. Bioaerosol deposition in single and two-bed hospital rooms: a numerical and experimental study. Build. Environ. 59, 436–447. http://dx.doi.org/10.1016/j.buildenv.2012.09.011.

Larsen, T.S., Heiselberg, P., 2008. Single-sided natural ventilation driven by wind pressure and temperature difference. Energy Build. 40, 1031–1040. http://dx.doi.org/10.1016/j.enbuild.2006.07.012.

Leonardi, S., Castro, I.P., 2010. Channel flow over large cube roughness: a direct numerical simulation study. J. Fluid Mech. 651, 519. http://dx.doi.org/10.1017/S002211200999423X.

Liddament, M., 1986. Air Infiltration Calculation Techniques – an Applications Guide. AIVC, Bracknell.

Liddament, M.W., 1996. A Guide to Energy Efficient Ventilation, first ed. (Coventry).

Lim, H.C., Thomas, T.G., Castro, I.P., 2009. Flow around a cube in a turbulent boundary layer: LES and experiment. J. Wind Eng. Ind. Aerodyn. 97, 96–109. http://dx.doi.org/10.1016/j.jweia.2009.01.001.

Lin, M., Hang, J., Li, Y., Luo, Z., Sandberg, M., 2014. Quantitative ventilation assessments of idealized urban canopy layers with various urban layouts and the same building packing density. Build. Environ. 79, 152–167. http://dx.doi.org/10.1016/j.buildenv.2014.05.008.

Menter, F.R., Egorov, Y., 2010. The scale-adaptive simulation method for unsteady turbulent flow predictions. part 1: theory and model description. Flow. Turbul. Combust. 85, 113–138. http://dx.doi.org/10.1007/s10494-010-9264-5.

Nozu, T., Tamura, T., Okuda, Y., Sanada, S., 2008. LES of the flow and building wall pressures in the center of Tokyo. J. Wind Eng. Ind. Aerodyn. 96, 1762–1773. http://dx.doi.org/10.1016/j.jweia.2008.02.028.

Perén, J.I., van Hooff, T., Leite, B.C.C., Blocken, B., 2015. CFD analysis of cross-ventilation of a generic isolated building with asymmetric opening positions: impact of roof angle and opening location. Build. Environ. 85, 263–276. http://dx.doi.org/10.1016/j.buildenv.2014.12.007.

Rahman, M., Biswas, R., Mahfuz, W., 2010. Effects of beta ratio and Reynold's number on coefficient of discharge of orifice meter. J. Agric. Rural. Dev. 7, 151–156. http://dx.doi.org/10.3329/jard.v7i1.4436.

Richards, P., Hoxey, R., Short, L., 2001. Wind pressures on a 6 m cube. J. Wind Eng. Ind. Aerodyn. 89, 1553–1564.

Richards, P.J., Hoxey, R., Connell, B.D., Lander, D.P., 2007. Wind-tunnel modelling of the Silsoe cube. J. Wind Eng. Ind. Aerodyn. 95, 1384–1399. http://dx.doi.org/10.1016/j.jweia.2007.02.005.

Richards, P.J., Hoxey, R.P., 2012. Pressures on a cubic building-Part 1: full-scale results. J. Wind Eng. Ind. Aerodyn. 102, 72–86. http://dx.doi.org/10.1016/j.jweia.2011.11.004.

Richards, P.J., Hoxey, R.P., 2006. Flow reattachment on the roof of a 6 m cube. J. Wind Eng. Ind. Aerodyn. 94, 77–99. http://dx.doi.org/10.1016/j.jweia.2005.12.002.

Richards, P.J., Hoxey, R.P., 2002. Unsteady flow on the sides of a 6 m cube. J. Wind Eng. Ind. Aerodyn. 90, 1855–1866. http://dx.doi.org/10.1016/S0167-6105(02)00293-3.

Richards, P.J., Norris, S.E., 2011. Appropriate boundary conditions for computational wind engineering models revisited. J. Wind Eng. Ind. Aerodyn. 99, 257–266. http://dx.doi.org/10.1016/j.jweia.2010.12.008.

Roache, P.J., 1997. Quantification of uncertainty in computational fluid dynamics. Annu. Rev. Fluid Mech. 29, 123–160. http://dx.doi.org/10.1146/annurev.fluid.29.1.123.

Sandberg, M., Sjöberg, M., 1983. The use of moments for assessing air quality in ventilated rooms. Build. Environ. 18, 181–197. http://dx.doi.org/10.1016/0360-1323(83)90026-4.

Sawachi, T., Ken-ichi, N., Kiyota, N., Seto, H., Nishizawa, S., Ishikawa, Y., 2004. Wind pressure and air flow in a full-scale building model under cross ventilation. Int. J. Vent. 2, 343–357. http://dx.doi.org/10.1080/14733315.2004.11683677.

Schwer, L.E., 2008. In: Is Your Mesh Good Enough? Estimating Discretization Error Using GCI. LS-DYNA Anwenderforum, Bamberg, pp. 45–54.

Spalart, P., 2000. Strategies for turbulence modelling and simulations. Int. J. Heat. Fluid Flow. 21, 252–263. http://dx.doi.org/10.1016/S0142-727X(00)00007-2.

Straw, M.P., 2000. Computation and Measurement of Wind Induced Ventilation. University of Nottingham.

Straw, M., Baker, C., Robertson, A., 2000. Experimental measurements and computations of the wind-induced ventilation of a cubic structure. J. Wind Eng. Ind. Aerodyn. 88, 213–230. http://dx.doi.org/10.1016/S0167-6105(00)00050-7.

Sundell, J., Levin, H., Nazaroff, W.W., Cain, W.S., Fisk, W.J., Grimsrud, D.T., Gyntelberg, F., Li, Y., Persily, A.K., Pickering, A.C., Samet, J.M., Spengler, J.D., Taylor, S.T., Weschler, C.J., 2011. Ventilation rates and health: multidisciplinary review of the scientific literature. Indoor Air 21, 191–204. http://dx.doi.org/10.1111/j.1600-0668.2010.00703.x.

Tominaga, Y., Blocken, B., 2016. Wind tunnel analysis of flow and dispersion in cross-ventilated isolated buildings: impact of opening positions. J. Wind Eng. Ind. Aerodyn. 155, 74–88. http://dx.doi.org/10.1016/j.jweia.2016.05.007.

Tominaga, Y., Blocken, B., 2015. Wind tunnel experiments on cross-ventilation flow of a generic building with contaminant dispersion in unsheltered and sheltered conditions. Build. Environ. 92, 452–461. http://dx.doi.org/10.1016/j.buildenv.2015.05.026.

Tominaga, Y., Stathopoulos, T., 2011. CFD modeling of pollution dispersion in a street canyon: Comparison between LES and RANS. J. Wind Eng. Ind. Aerodyn. 99, 340–348. http://dx.doi.org/10.1016/j.jweia.2010.12.005.

Tominaga, Y., Mochida, A., Murakami, S., Sawaki, S., 2008. Comparison of various revised k-ε models and LES applied to flow around a high-rise building model with 1:1:2 shape placed within the surface boundary layer. J. Wind Eng. Ind. Aerodyn. 96, 389–411. http://dx.doi.org/10.1016/j.jweia.2008.01.004.

van Hooff, T., Blocken, B., Tominaga, Y., 2017. On the accuracy of CFD simulations of cross-ventilation flows for a generic isolated building: comparison of RANS, LES and

experiments. Build. Environ. 114, 148–165. http://dx.doi.org/10.1016/j.buildenv.2016.12.019.

Wang, A., Zhang, Y., Sun, Y., Wang, X., 2008. Experimental study of ventilation effectiveness and air velocity distribution in an aircraft cabin mockup. Build. Environ. 43, 337–343. http://dx.doi.org/10.1016/j.buildenv.2006.02.024.

Wen, C.-Y., Juan, Y.-H., Yang, A.-S., 2017. Enhancement of city breathability with half open spaces in ideal urban street canyons. Build. Environ. 112, 322–336. http://dx.doi.org/10.1016/j.buildenv.2016.11.048.

Xie, Z.-T., Castro, I.P., 2009. Large-eddy simulation for flow and dispersion in urban streets. Atmos. Environ. 43, 2174–2185. http://dx.doi.org/10.1016/j.atmosenv.2009.01.016.

Xie, Z., Castro, I.P., 2006a. LES and RANS for turbulent flow over arrays of wall-mounted obstacles. Flow. Turbul. Combust. 76, 291–312. http://dx.doi.org/10.1007/s10494-006-9018-6.

Xie, Z., Castro, I.P., 2006b. Large-eddy simulation for urban micro-meteorology. J. Hydrodyn. Ser. B 18, 259–264. http://dx.doi.org/10.1016/S1001-6058(06)60062-0.

Yang, T., 2004. CFD and Field Testing of a Naturally Ventilated Full-scale Building. University of Nottingham.

Yu, H., Thé, J., 2016. Validation and optimization of SST k-ω turbulence model for pollutant dispersion within a building array. Atmos. Environ. 145, 225–238. http://dx.doi.org/10.1016/j.atmosenv.2016.09.043.